

III-5

Life, Earth and
Planetary Sciences





BL3U

X-ray Absorption Spectra of Lipid Bilayer Membranes in Aqueous Solutions

R. Tero¹, Yu Kinjo¹ and M. Nagasaka²¹Toyohashi University of Technology, Toyohashi, 441-8580, Japan²Institute for Molecular Science, Okazaki 444-8585, Japan

The lipid bilayer is a self-assembled structure of amphiphilic lipid molecules. It is the fundamental structure of biomembranes such as cell membranes, which are the fields for the transportation of materials, information, and energy into and out of cells. All these physiological reactions proceed in the presence of electrolytes. Ions in the aqueous solution significantly influence to physical properties and structures of lipid bilayers. Phosphatidylcholine (PC) is the most abundant lipid of eukaryotic cell membranes. Cations bind to the phosphate and carbonyl groups of PC. However, affinity of cations to PC and effects of cations to molecular orientation are still controversy especially in the fields of theoretical simulations. We aim to determine the binding affinity of cations to lipids in aqueous solutions experimentally, by means of X-ray absorption spectroscopy (XAS) [1, 2].

Supported lipid bilayers (SLBs) of dioleoyl-PC (DOPC) were formed on the Si_3N_4 membranes of the XAS flow cell [1] by the vesicle fusion method in a buffer solution (NaCl 100 mM, HEPES 25 mM/ pH 7.4 NaOH). The Na^+ concentration ($[\text{Na}^+]$) was varied by exchanging the buffer solution in the flow cell in the range of $[\text{Na}^+] = 2.1 - 510.4$ mM. The O-K edge XAS spectra of SLB were obtained at the energy range of 527 – 535 eV at the Xray incident angle of 35° . The XAS spectrum of the Si_3N_4 membrane without SLB was subtracted from that with SLB.

The O-K-edge spectrum of DOPC appeared at 531 – 533 eV (Fig. 1). It is consisted of $1s \rightarrow \pi^*$ transitions of double-bond oxygens in the phosphate and carbonyl groups on the PC headgroup: two components attributed to the P=O in the former, and one component attributed to the latter [3]. We measured XAS spectra at the X-ray incident angle (T) of 35° to obtain the intensity of each component independently of the molecular orientation. We obtained a specific dependence of the P=O peak at the lower energy (P=O_{low}) on $[\text{Na}^+]$: its position was identical at $[\text{Na}^+] = 2.1 - 10.4$ mM, shifted to higher energy by 0.4 eV above $[\text{Na}^+] = 10.4$ mM, and little independent of $[\text{Na}^+]$ above 110.4 mM. The results show the Na^+ coordination to the phosphate group of PC and its dependence of $[\text{Na}^+]$. The inner-shell quantum chemical calculation [4] of O K-edge spectrum of P=O indicated that coordination of Na^+ to the phosphate group causes higher-energy shift of P=O peaks. The dependence of the P=O peak intensity as well as the P=O intensity on $[\text{Na}^+]$ is investigated in

detail. The effects of the cation species on the XAS components will be investigated.

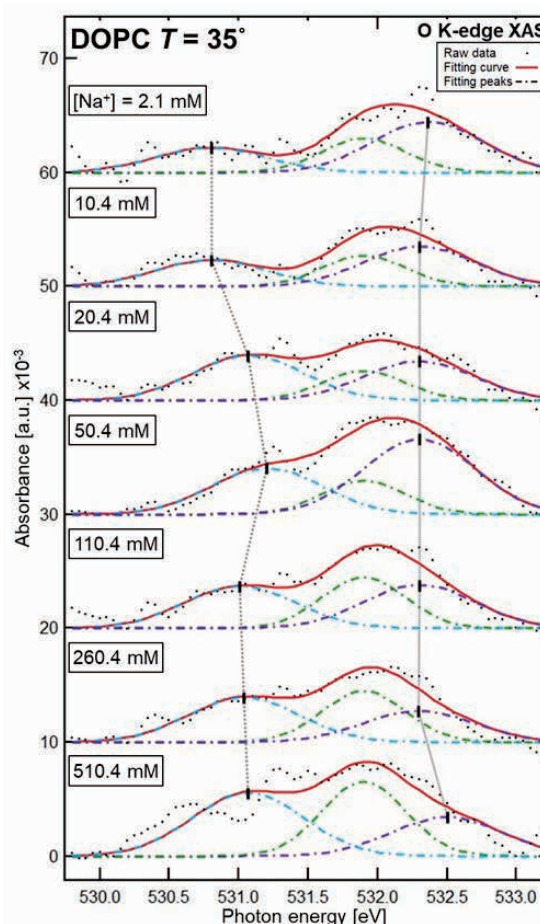


Fig. 1. O K-edge XAS spectra of DOPC-SLB at $[\text{Na}^+] = 2.1 - 510.4$ mM obtained at the X-ray incident angle of 35° . Black dotted curves represent raw data. Dashed curves and red solid curves show deconvoluted components and their summation, respectively.

- [1] M. Nagasaka, H. Yuzawa, T. Horigome, and N. Kosugi, *J. Electron Spectros. Relat. Phenomena* **224** (2018) 93.
- [2] R. Tero, Y. Kinjo and M. Nagasaka, *UVSOR Activity Report* **49** (2021) 151.
- [3] R. Tero, W.-Z. Goh and M. Nagasaka, *UVSOR Activity Report* **48** (2020) 129.
- [4] M. Nagasaka, *J. Chem. Phys.* **158** (2023) 024501.

Study on Chirality Emergence of Amino Acid Molecules Induced by Circularly Polarized Lyman- α Light Irradiation

M. Kobayashi¹, J. Takahashi², H. Ota³, G. Fujimori², K. Kobayashi², K. Matsuo⁴, Y. Taira³,
M. Katoh^{3,4}, H. Nakamura¹ and Y. Kebukawa²

¹National Institute for Fusion Science, 322-6 Oroshi-cho, Toki 509-5292, Japan

²Yokohama National University, 79-5 Tokiwadai, Hodogaya-ku, Yokohama 240-8501, Japan

³UVSOR Synchrotron Facility, Institute for Molecular Science, Myodaiji, Okazaki 444-8585, Japan

⁴Hiroshima Synchrotron Radiation Center, Hiroshima University, 2-313 Kagamiyama, Higashi-Hiroshima 739-0046, Japan

The origin of homochirality in terrestrial biomolecules (L-amino acid and D-sugar dominant) remains one of the most mysterious problems in the research for the origins of life. One of the most attractive hypotheses in the context of astrobiology is “Cosmic Scenario” [1, 2]; Asymmetric reactions of prebiotic molecules on interstellar dust surfaces in molecular cloud circumstances were introduced by polarized quantum radiation sources in space, that is “chiral radiations”. Among the polarized quantum radiation sources, circularly polarized light (CPL) in the space environment is thought to be one of the most likely causes of the enantiomeric excesses of terrestrial bioorganic molecules. In this study, we focused on a hydrogen Lyman- α wavelength of 121.6 nm, where strong emission lines are observed in star-forming regions.

Alanine is selected as a chiral prebiotic molecules in the interstellar space. We formed thin solid film samples of racemic mixture of alanine (DL-alanine) on quartz substrates from crystal powders of DL-alanine by using a thermal-crucible vacuum-evaporation system at HiSOR in Hiroshima university. A schematic of the irradiation system of BL1U is shown in Fig.1. The 121.6 nm wavelength radiation from the undulator is reflected by a gold-coated mirror (M0 focusing mirror) located in the mirror chamber directly beam upstream of the irradiation chamber and then enters the irradiation chamber. On the beam entrance side of the vacuum sample chamber, a gate valve with an MgF2 vacuum sealing window (0.5 mm in thickness) was mounted. The use of gold-coated mirror reflections has made it possible to suppress high-energy higher order light from the undulator source, expecting to reduce the transmittance loss of the MgF2 window due to high-energy radiation induced defects. The sample substrate was set in the sample holder in the irradiation chamber, in which magnetic and electric fields can be applied to perpendicularly to the sample surface. The total photon beam intensity irradiated on the sample was monitored with photoelectron current of a silicon photodiode settled at the beam downstream side of the sample holder.

CD spectra of the CPL irradiated films were measured using the SR-CD beam line BL-12 of HiSOR to clarify

the optical activity emergence by CPL irradiation. Figure 2(a) shows spectra of DL-alanine films irradiated for 30 min with L- or R-CPL at 121.6 nm in wavelength. We clearly observe optical activity induced by the CPL irradiation, which shows opposite sign in the CD between right CPL and left CPL. In addition, we have also examined the additional effect of applying a magnetic field to the sample to investigate the effect of the magnetic field in interstellar space (Fig. 2(b)). The application of the magnetic field seems to alter the CD spectra, suggesting a certain impact of symmetry breaking of the optical activity caused by the CPL irradiation. Detailed analysis of CD spectra is in progress supported by quantum chemical calculations.

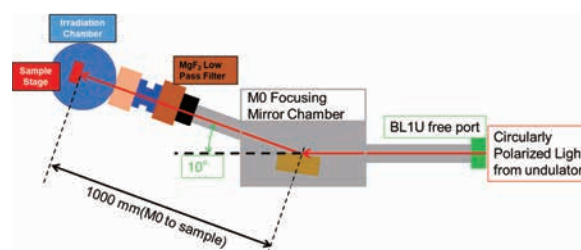


Fig. 1. A schematic of the CPL irradiation system at BL1U.

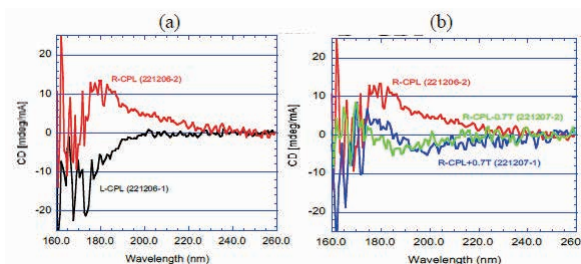


Fig. 2. CD spectra of alanine sample after irradiation of (a) right (red) and left (black)-CPL, and (b) right CPL with magnetic field application (blue:+0.7T, green:-0.7T).

[1] W. A. Bonner, Orig. Life Evol. Biosph. **21** (1991) 407.

[2] J. Takahashi and K. Kobayashi, Symmetry **11** (2019) 919.

BL3U

Attempts at Structural Analysis of Biological Macromolecules Using Resonant Soft X-ray Scattering

Y. Sugimoto¹ and H. Iwayama^{1,2}

¹UVSOR Synchrotron Facility, Institute for Molecular Science, Okazaki 444-8585, Japan
²School of Physical Sciences, The Graduate University for Advanced Studies (SOKENDAI), Okazaki 444-8585, Japan

Resonant soft X-ray scattering (RSoXS) is a powerful technique to probe the nano-to-mesoscopic structure of molecules. Since this method observes scattered waves due to resonance processes, RSoXS can reveal structures with enhanced or tunable scattering contrast. In particular, since soft X-ray regions include K-edge energies of light elements such as carbon, nitrogen, and oxygen, RSoXS is a suitable tool for investigating soft matters. In UVSOR, the development of the RSoXS instrument has begun since 2019, and we have successfully measured the mesoscopic structure of liquid crystal molecules [1].

Biomacromolecules, such as proteins, are also mainly composed of light-element atoms. Studying biomacromolecule structures is crucial for elucidating biological functions and developing therapeutic drugs. Conventional electron microscopy (EM) and small-angle X-ray scattering (SAXS) are well-established methods for investigating the structure of biological macromolecules. The RSoXS method is expected to complement conventional methods due to its features, such as the selectivity of elements and functional group orientations. In this work, we performed RSoXS measurements for protein samples.

Our RSoXS measurements were performed at UVSOR BL3U. Our sample is bovine milk casein as the typical protein sample. Casein forms micelles with calcium phosphate dispersed inside [2]. We prepared the bovine milk samples in the following step. First, we dissolved the bovine milk powder sample in water, then dropped samples onto a Si_3N_4 membrane and dried them naturally. We set the samples in the vacuum chamber and irradiated them with soft X-rays. We measured the scattering intensity with a soft X-ray CCD camera (Andor BN940P). The photon energies were set to 270, 285, 348, and 350 eV. The measured Q-range was $0.035\text{--}0.35\text{ nm}^{-1}$ at 270 eV and $0.055\text{--}0.45\text{ nm}^{-1}$ at 350 eV. The Guinier plot of the scattering intensity yields the radius of gyration of $\sim 55\text{ nm}$,

measured at 270 eV below the carbon K-edge absorption. This value is close to the structure of casein micelles obtained in previous studies. The scattering intensity measured at 350 eV, near the calcium L absorption edge, showed a different scattering intensity than that at 348 eV (Fig. 1). The resonance-enhanced structure of the spectrum suggests that RSoXS gives insight into a more detailed structure of calcium phosphate in casein micelles, compared to conventional SAXS.

On the other hand, some structural changes in biomolecules may come from the drying process of the sample preparations. In addition, our equipment is difficult to measure small scattering-angle regions due to the direct beam. We will introduce a new sample cell for wet samples and improve our RSoXS spectrometer for small scattering angle measurements.

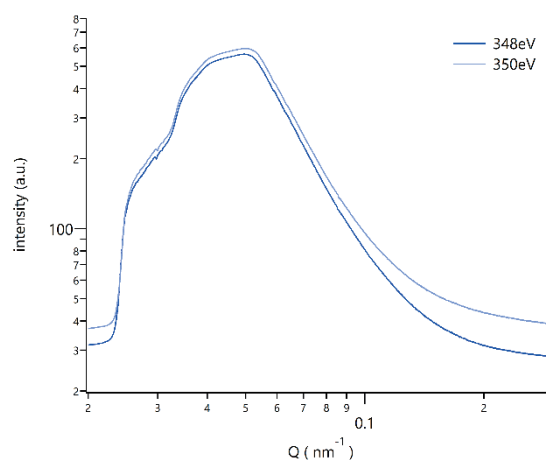


Fig. 1. Q-spectra for casein at the calcium L absorption edge.

- [1] Y. Takanishi *et al.*, RSC Adv. **12** (2022) 29346.
 [2] H. Takagi *et al.*, Food Chem. **393** (2022) 133389.

Water-Ion Interactions in Natural Lake Brines

Y. Hao¹, N. Fauré², Y. Qiu¹, M. Nagasaka³, E. Thomson², S. Wang¹ and X. Kong²

¹Department of Environmental Sciences, College of Urban and Environmental Sciences, Northwest University, Xi'an, China

²Department of Chemistry and Molecular Biology, Atmospheric Science, University of Gothenburg, SE-412 96 Gothenburg, Sweden

³Institute for Molecular Science, Okazaki 444-8585, Japan

Under climate change and enhanced water use demands, arid regions are undergoing faster transformations compared to humid areas due to their greater susceptibility to changes in precipitation. As a consequence, the number and area of saline lakes are being impacted. Depending on the local circumstances, some saline lakes are being desiccated and transforming to playa covered by evaporite salts, while others are forming and expanding, such as the lakes in the Qinghai-Tibet Plateau [1]. The increases volume and surface area of saline lakes are expected to have impacts on local environment and climate.

In this beamtime, we carried out Near Edge X-ray Absorption Fine Structure (NEXAFS) measurements on brines from various saline lakes in the Qaidam Basin, which is situated in the Qinghai-Tibet Plateau. The sampling sites include eight saline lakes: Mang'ai Feicui Lake (MA), Dalangtan Playa (DLT), West Taijinar Lake (XT), East Taijinar Lake (DT), Qarhan Lake (QH), Dezongmahai Lake (DZMH), Dachaidan Lake (DCD), and Xiaochaidan Lake (XCD) (Figure 1). The brine samples were taken 2 – 5 cm below the lake surface, and then were stored in polyethylene bottles, sealed with Parafilm membranes, and stored at 4 °C.

The NEXAFS measurements were performed at the soft X-ray undulator beamline BL3U at UVSOR-III Synchrotron. In the liquid flow cell, a liquid layer is sandwiched between two 100 nm thick Si₃N₄ membranes with the windows size of 2 × 2 mm². Teflon spacers with the thickness of 100 μm are set between the support plates of the Si₃N₄ membranes. Liquid samples are exchangeable *in situ* by using a tubing pump. The temperature of all the liquid samples were controlled at approx. 25 °C. The Si₃N₄ membrane window was set to 200 × 200 μm² to allow for suitable photon fluxes.

In Figure 2, the O K-edge NEXAFS results are presented, with 8 brines displayed in two panels for better visibility. The pure water case is also included in both panels for comparison purposes. The spectra exhibit three features: pre-edge (~535 eV), main-edge (~537 eV), and post-edge (~540 eV), with the spectrum lines normalized to the maximum at the main-edge. The post-edge intensities of the brines are lower than those of pure water, which is consistent with existing literature [2]. The pre-edges have been zoomed in and displayed in the insets. Apart from the DZMH brine, the other brines exhibit reduced and shifted pre-edge

peaks, which will be analyzed in more detail. The DZMH brine displays a notably high pre-edge, likely resulting from contamination.

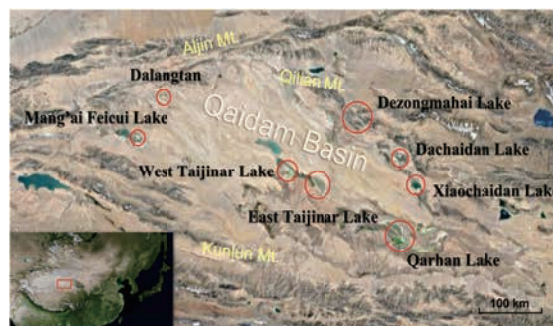


Fig. 1. Eight saline lakes, as marked by red circles, were sampled in the Qaidam Basin.

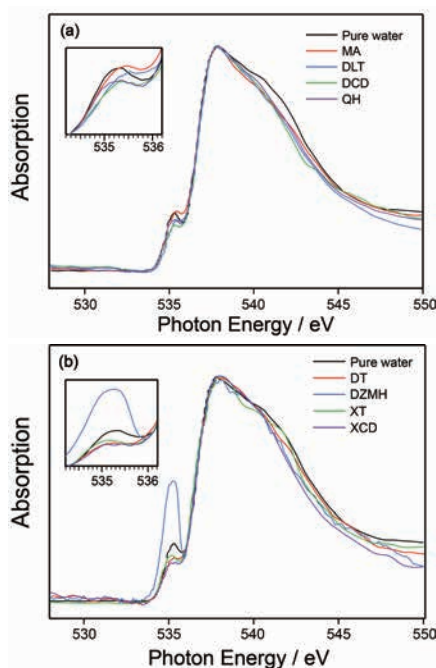


Fig. 2. O K-edge NEXAFS spectra of (a) pure water and brines from MA, DLT, DCD, and QH lakes; (b) pure water and brines from DT, DZMH, XT, and XCD lakes. The temperatures are around 25 °C. The insets zoom in the pre-edge regions.

[1] Zhang, G. *et al.*, *Earth Sci. Rev.* **208** (2020) 103269.

[2] Nagasaka, *et al.*, *J. Phys. Chem. B*, **121** (2017) 10957-10964.

BL4U

Drug Administration Concepts Involving Redox Nanocarriers Affect the Spatial Distribution of Topically Applied Formulations in Human Skin

G. Germer¹, T. Ohgashi², H. Yuzawa², K. Rajes³, R. Haag³, F. Rancan⁴, A. Vogt⁴ and E. Rühl¹

¹Physical Chemistry, Freie Universität Berlin, Arnimallee 22, 14195 Berlin, Germany

²UVSOR Synchrotron Facility, Institute for Molecular Science, Okazaki 444-8585, Japan

³Organic Chemistry, Freie Universität Berlin, Arnimallee 22, 14195 Berlin, Germany

⁴Charité Universitätsmedizin, 10117 Berlin, Germany

Different drug administration concepts involving redox-sensitive polymer nanocarriers topically applied to human skin *ex vivo* have been investigated by scanning transmission X-ray microscopy (STXM). The goal of this research is to understand how single and repeated use of drug formulations containing nanocarriers affects the drug and nanocarrier distribution in the top skin layers of inflamed skin. Especially, the repeated use of drug formulations is frequently used in therapy. STXM probes sensitively and label-free the distribution of topically applied formulations [1]. The results are of importance to understand the transport and penetration routes of actives. Polymer nanocarriers are used for transporting drugs that are barely penetrating the skin barriers [2, 3]. The present studies compare different topical drug delivery concepts of a single dose and repeated drug administrations, reaching up to five days, respectively. The skin barrier was initially modified for all samples by topically applying the oxidizer di-benzoyl peroxide (DBPO) for 16 h prior to topical application of rapamycin-loaded oxidation-sensitive nanocarriers (osCMS [2]). The osCMS samples (5 mg/mL, $\leq 2\%$ drug loading) were formulated in HEC gel. $40 \mu\text{L}/\text{cm}^2$ of this formulation were applied once for up to 1000 min to the skin samples *ex vivo*. In case of repeated treatments, the skin was four times treated every 24 h with $40 \mu\text{L}/\text{cm}^2$ of a 1% rapamycin-osCMS formulation with a final drug concentration of $8 \mu\text{g}/\text{cm}^2$. The STXM experiments were performed at the BL4U beamline of UVSOR III at the O 1s regime (520 – 565 eV). Key is the acquisition of stacks of images by concentrating on the top skin layers, i.e., the stratum corneum (SC) and the viable epidermis (VE). Fig. 1 shows selected results, where a comparison is made between the single treatment (Fig. 1(a)) and multiple treatments (Fig. 1(b)). At the top of each Figure an X-ray micrograph recorded at 532 eV is shown, indicating the skin structure of the vertical cuts of EPON-fixed skin, where the skin surface is located at the right hand side. Each Figure also contains the local concentrations of rapamycin ① and osCMS ②, derived from the experimental results and subsequent singular value decomposition, similar to recent work [1]. Single treatment shows primarily the species of interest in the stratum corneum (Fig. 1(a)), where the nanocarriers are

mostly found in narrow spatial distribution in the lipids separating the corneocytes, whereas the drug is found in the corneocytes. Multiple treatments (Fig. 1(b)) show a different distribution of both species: Most of the drug has been transported in deeper skin layers, only some of the rapamycin remains in corneocytes. Nanocarriers are primarily found in the viable epidermis, and there they are localized near the cell nuclei. This deep penetration of osCMS into the viable parts of skin is likely the result of a damaged tight junction barrier in the stratum granulosum due to initial treatment by DBPO, as nanocarriers were not observed before in the viable parts of intact skin after single treatment [3]. These differences in drug and nanocarrier distributions provide evidence that in inflamed skin the drug is efficiently transported via nanocarriers to the sites of action, where it is needed for therapeutic success, considering that the drug dissolved in ethanol is barely taken up by intact skin [1].

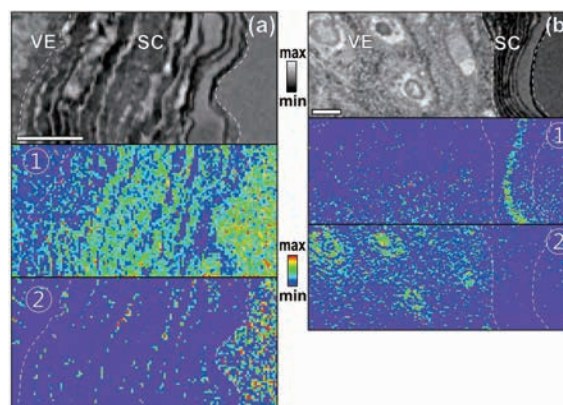


Fig. 1. Results from STXM on different drug delivery concepts of human skin *ex vivo* initially treated by DBPO: (a) single drug application (1000 min); (b) repeated use of drug administration (5 d). Top: X-ray micrograph recorded at 532 eV, below: local concentrations of ① rapamycin and ② osCMS. Scale bar: 5 μm .

[1] G. Germer *et al.*, ACS Omega **6** (2021) 12213.

[2] K. Rajes *et al.*, Pharmaceutics **13** (2021) 37; K. Rajes *et al.*, Biomater. Sci. Engin. **7** (2021) 2458.

[3] K. Yamamoto *et al.*, J. Control. Release **242** (2016) 64.

Absorption- Image and Spectra of Apoptosis Nuclei in P-L Edge

T. Ejima¹ and S. Tone²

¹SRIS, Tohoku University, Sendai 980-8577, Japan

²Sch. of Sci & Technol., Tokyo Denki University, Hatoyama 350-0394, Japan

Apoptosis is programmed death of cells that is an important physiological function for the recycling of cellular components and characterized by chromatin condensation in the cell nucleus. Detailed studies of the chromatin condensation process in isolated cell nuclei have shown that this condensation process occurs in three stages from the normal state of the cell nucleus (Stage 0) to ring condensation (Stage 1), necklace condensation (Stage 2), and cell nuclear collapse/disassembly (Stage 3) [1]. It has been suggested that among the transitions from Stage 0 to 3, Stage 1 to 2 is caused by cleavage of phosphodiester bonds in DNA, while protein kinases such as MST1 may be the cohesive factor in the transition from Stage 2 to 3 [1].

To investigate the change from Stage 0 to Stage 1, infrared absorption experiments were performed, focusing especially on the change in the vibrational structure of PO_2^- , which is sensitive to the helical structure of DNA. As a result, the helical structure, which was predominantly B-DNA in Stage 0, decreased as the step progressed, and changed to A-DNA or Z-DNA. This result suggests that the helical structure of DNA changes from Stage 0 to 1, DNA is cleaved in Stage 1 to 2, and phosphate groups are transferred from DNA in Stage 2 to 3. In this study, we focused on this change in the phosphate group of DNA and thought that we could capture the changes in DNA at each stage by measuring the P-L_{2,3} absorption edge structure of the cell nucleus.

The samples used in the experiments were obtained according to the method reported by Tone et al [1]. The isolated nuclei of each stage obtained were embedded and sectioned into approximately 100 nm-thick section samples using an ultramicrotome. The sectioned samples were imaged under an optical microscope and cell nuclei showing representative shapes of each stage were selected in the images. Isolated nuclei of Stage 0 and Stage 2 were selected for measurement due to time limitations, and STXM measurements of the C-K and P-L absorption edges were performed for each. The obtained STXM images were analyzed by PCA and reconstructed after removing noise components from the PCA component images, and cluster analysis was performed to the reconstructed images [2]. Figure shows the STXM image of a Stage 2 isolated nucleus at the P-L absorption edge and the obtained absorption spectrum. The spectra show two peak structures, P-L₂ and L₃, split by spin-orbit interaction. We believe that

the spectral shape of each peak is similar to that of PO_4 . In combination with the image, it is considered that DNA was degraded and transformed into PO_4 clusters as apoptosis progressed. This interpretation is consistent with the result of IR absorption results.

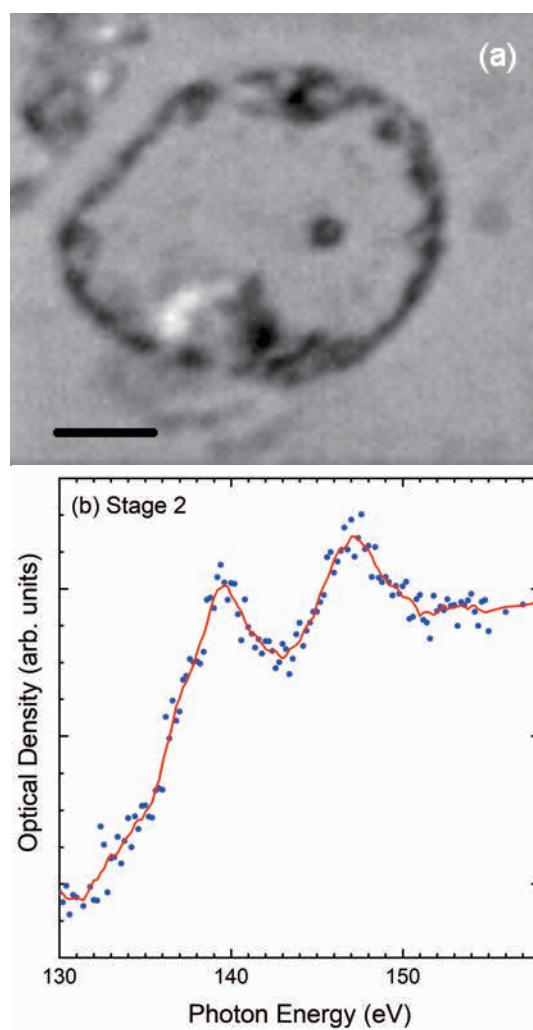


Fig. 1. X-ray absorption image, (a), and X-ray absorption spectrum, (b), of apoptosis nucleus in stage2 at P-L absorption edge. Bar is 2 μm in length.

References:

- [1] S. Tone *et al.*, *Exp. Cell Res.* **313** (2007) 3635.
- [2] M. Lerotic *et al.*, *JESRP* **144-147** (2005) 1137.

BL4U

Embracing Natural and Anthropogenic Aerosol Particle Complexity

P. A. Alpert¹, L. Li², L. F. Escusa Dos Santos², F. Mahr¹, M. Ammann¹, L. Wu³, W. Hu³,
P. Fu³, M. Hallquist², E. Thomson² and X. Kong²

¹Laboratory for Environmental Chemistry, Paul Scherrer Institute, Villigen PSI, 5232, Switzerland

²Atmospheric Science Research Group, Department of Chemistry and Molecular Biology,
University of Gothenburg, 41296 Gothenburg, Sweden

³School of Earth Systems Science, Tianjin University, 300072 Tianjin, China

A considerable fraction of the global population lives in coastal urban centers. People in these regions are exposed to some of the most complex aerosol particles containing mixtures of natural and anthropogenic compounds. The chemical composition and morphology of these particles are key for their environmental impacts, but remain poorly understood. We have investigated particles taken from ambient air that was influenced by the ocean and mixed ocean-anthropogenic sources to better understand their cloud-forming potential, chemical reactivity and light-scattering properties.

Sea spray aerosol particles contain sea-salts and organic matter [1]. When mixed with anthropogenic air, these particles can uniquely undergo acid displacement reactions forming organic salts and producing inorganic acids, which evaporate from the particles [2]. Mixed anthropogenic and natural aerosol particles aerosolized from saline lakes have previously been shown to act as cloud nuclei [3]. Additionally, anthropogenic emissions from ships are known to have a variable ability to nucleate clouds depending on the type of fuel used and its sulfur content [4].

To better understand such complex processes we collected ambient particles from contrasting sources, *i*) the Indian Ocean with minimal anthropogenic influence, *ii*) the Indian Ocean with significant anthropogenic influence and *iii*) Sanya Port, a coastal city in China. At the Ultraviolet Synchrotron Orbital Radiation Facility, we probed individual particles at the carbon, oxygen and nitrogen K-edges, and the sulfur, chlorine and calcium L-edges using scanning transmission X-ray microscopy coupled to near-edge X-ray absorption fine structure spectroscopy (STXM/NEXAFS). We quantified how inorganics and organics were mixed in individual particles and determined the organic volume fraction (OVF) [5]. The OVF was calculated from high spatial resolution images at 280 eV, 285.4 eV, 288.7 eV and 320 eV with a pixel size of $0.05 \times 0.05 \mu\text{m}^2$.

Figure 1 shows optical density measured at 280 eV and OVF for the same field of view of Indian Ocean particles without anthropogenic influence. The optical density image shows X-ray absorption primarily due to elements that are not carbon, such as Na and Cl, as well as other sea salts and inorganic matter. Particle morphology is largely cubic with submicrometer sized

needle-like structures, as expected for sea spray aerosol particles. Based on our STXM/NEXAFS measurements, these needles were confirmed to be dominated by calcium sulfate. The OVF image reveals a considerable fraction of organic material close to salt cores. Carbon K-edge spectra were dominated by carboxyl functional groups, similar to sea spray aerosol particles found over various ocean environments [1, 2, 5].

These data suggest that these particles will likely be highly hygroscopic and act as cloud condensation and ice nuclei due to their high salt content and similar carbon spectra as other ice nucleating particles [1]. Additionally, morphology and composition determined from STXM/NEXAFS are similar to laboratory-generated ice nucleating sea spray particles, implying a role for atmospheric ice particle production [1]. The highest OVF appears close to the salt at values around 0.6 and decreases with distance away from the crystal. This implies a small degree of aging, i.e., that organic salts dominate likely due to acid displacement reaction rather than pure organic coatings. Further work is ongoing to identify differences in particles from various sources and their importance for cloud microphysics and aerosol chemistry.

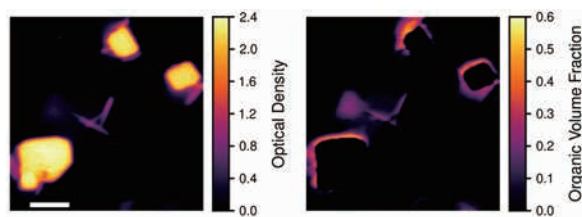


Fig. 1. Optical density at 280 eV indicating X-ray absorption primarily due to compounds other than carbon. Organic volume fraction of the same particles calculated for particles collected over the Indian Ocean. Scale bar is $2 \mu\text{m}$.

- [1]P. A. Alpert *et al.*, *Sci. Adv.* **8** (2022) eabq6842.
[2]A. Laskin *et al.*, *J. Geophys. Res.-Atmos.* **117** (2012) D15302.
[3]J. Li *et al.*, *Atmosphere* **12** (2021) 1203.
[4]L. F. E. d. Santos *et al.*, *Environ. Sci.: Atmos.* **3** (2023) 182.
[5]M. Fraund *et al.*, *Atmos. Meas. Tech.* **12** (2019) 1619.

STXM in Characterizing Lysosomal Storage Materials in a Mouse Model

T. Mansikkala^{1,2}, T. Ohigashi³, H. Yuzawa³, I. Miinalainen², S. M. Kangas⁴, M. Salo^{4,5},
N. Kosugi³, J. Uusimaa⁴, M. Huttula¹, R. Hinttala^{4,5} and M. Patanen^{1,2}

¹Nano and Molecular Systems Research Unit, PO Box 3000, 90014 University of Oulu, Finland

²Biocenter Oulu, PO Box 5000, 90014 University of Oulu, Finland

³UVSOR Synchrotron Facility, Institute for Molecular Science, Okazaki 444-8585, Japan

⁴Research Unit of Clinical Medicine and Medical Research Center, Oulu University Hospital and University of Oulu, 90014 Oulu, Finland

⁵Transgenic and Tissue Phenotyping Core Facility, University of Oulu, Finland

In this work, we used scanning transmission X-ray microscopy (STXM) technique at BL4U beamline to study lysosomal storage disease (LSD) mouse model liver and kidney tissues. LSDs are a large family of diseases where e.g. enzymatic dysfunction leads to accumulation of macromolecules in the tissues. This study was part of a project to better understand them. STXM hold promise to be a good tool to study LSDs if the natural chemical contrast of accumulating material and rest of the tissue is high enough. In our previous beamtimes at UVSOR both human and mouse model samples have been studied (Patanen 2018, Mansikkala 2020). This time our aim was to differentiate the storage material within the lysosomes. Liver and kidney tissue samples were used. They both had clear ultrastructural differences compared control samples in form of large number of vacuoles, presumed to be lysosomes fitting the description of the LSDs. Our preliminary studies showed a distinct spectrum from lysosomes compared to the rest of the tissue. This study was to verify the finding in larger number of samples.

The tissue samples were fixed in 4% paraformaldehyde and 2.5% glutaraldehyde in 0.1 M phosphate-buffered saline and then embedded in TTE:MMHA. The 150 nm thick sections were imaged with TEM to find areas with lysosomes on the samples. The same area was then measured with STXM from the subsequent thin sections.

We were able to find and image lysosomes in both tissue types, an example shown in Fig. 1. When analyzing the samples with aXis2000, we noticed that the spectrum from the lysosomes was very similar to that of the TTE:MMHA resin (Fig. 2). To evaluate the result, we subtracted the measured pure resin spectrum from the measured lysosome spectrum shown in Fig. 3 (green). There is only a small peak around 289 eV differentiates the lysosome spectrum from a resin spectrum. However, the spectrum from the extracellular space (blue) is almost identical with just intensity differences. The spectrum of cytosol differs clearly, indicating that the contents of the lysosomes are mostly TTE:MMHA resin. While there is a small difference between the resin and lysosomes and extra cellular space, the spectra are overwhelmed by the resin signal, and we were not able to differentiate the accumulation material spectrum in the lysosomes. Our hypothesis is that the sample preparation has substituted the accumulation material in lysosomes with resin instead of preserving it.

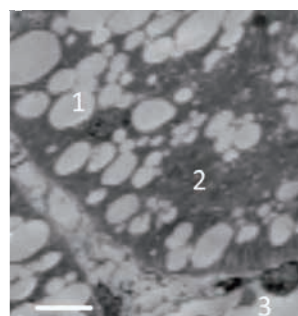


Fig. 1. STXM image of disease model mouse kidney with visible ultrastructural changes. Lysosomes are marked with 1, cytosol with 2 and extracellular space with 3. Scale bar is 5 μ m.

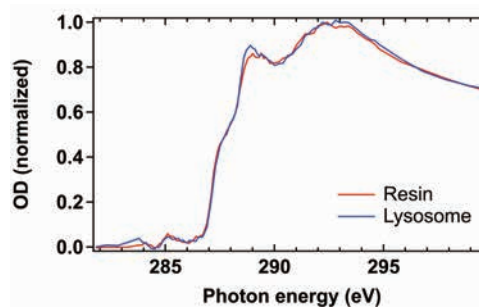


Fig. 2. Comparison of spectra from lysosome (blue) and pure resin (red).

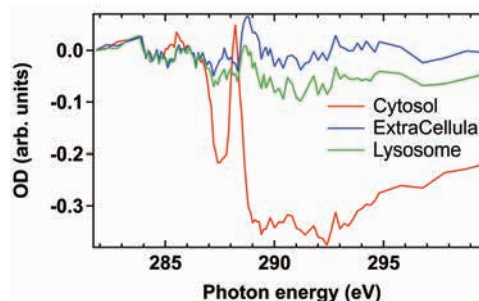


Fig. 3. Spectra from lysosome (green), the extracellular space (blue) and cytosol (red).

[1] T. Mansikkala *et al.*, *UVSOR Activity report 2019* (2020) 155.

[2] M Patanen *et al.*, *UVSOR Activity report 2018* (2019) 166.

BL4U

Determination of Spectral Changes in NEXAFS of Biomolecules Caused by Radiation Effects for Molecular Mapping of Biological Specimens

A. Ito¹, K. Shinohara², A. Matsuura³, S. Toné⁴, K. Tohya⁵, H. Yuzawa⁶ and T. Ohigashi^{6,7}

¹School of Engineering, Tokai University, Hiratsuka 259-1292, Japan

²Graduate School of Health Sciences, Fujita Health University, Toyoake, 470-1192, Japan

³Research Integrity Office, Fujita Health University, Toyoake, 470-1192, Japan

⁴School of Science and Engineering, Tokyo Denki University, Hatoyama, 350-0394, Japan

⁵Kansai University of Health Sciences, Kumatoricho, 590-0482, Japan

⁶UVSOR Synchrotron Facility, Institute for Molecular Science, Okazaki 444-8585, Japan

⁷School of Physical Sciences, The Graduate University for Advanced Studies, Okazaki 444-8585, Japan

We have been working on a quantitative mapping of nucleic acids (DNA and RNA) and proteins (histone and bovine serum albumin abbreviated as BSA) in chromosomes, cultured mammalian cells, and isolated apoptotic nuclei using combined NEXAFS spectra at the C, N and O *K*-edges [1-3]. The molecular mapping is based on the NEXAFS profiles of constituent biomolecules obtained independently. However, increased exposure dose required for X-ray imaging will modify NEXAFS profiles of biomolecules as reported previously [4]. For the precise molecular mapping of biological specimens, spectra measured at the same exposure as that used in the specimen imaging are required. Furthermore, the knowledge of the exposure dependence of NEXAFS profiles would improve the reliability of molecular mapping of biological specimens whose images are taken at any exposure time.

In our previous report, we detected a slight change of NEXAFS profiles of DNA at C, N and O *K*-edges, depending on the exposure time [4]. In the present study, we extended our analysis to the absorbed dose dependence of the mass absorption coefficient for all the energy points of NEXAFS, where absorbed dose is calculated from the exposure.

We prepared dry thin films of DNA, RNA, histone, BSA, actin, actin monomer and nucleosome on SiN membrane. Each one micrometer square area in the specimens was scanned with 10 x 10 pixels at the energy of C, N and O *K*-edge regions mainly in this order with a dwell time of 6, 12 and 20 msec in addition to 2 msec for DNA. For each dwell time the scanned area was shifted to the different area to avoid additional radiation effects to molecules.

Examples of the absorbed dose dependence of mass absorption coefficient are shown in Figure 1 at the lowest energies in the NEXAFS measurements of DNA at the C, N and O *K*-edges. All data in the repeated experiments for several times were compiled in the figures. The linear regression lines showed a slight decrease with increasing absorbed dose, which means that radiation affects the spectra of molecules. Estimation of NEXAFS profiles at a given absorbed dose is in progress.

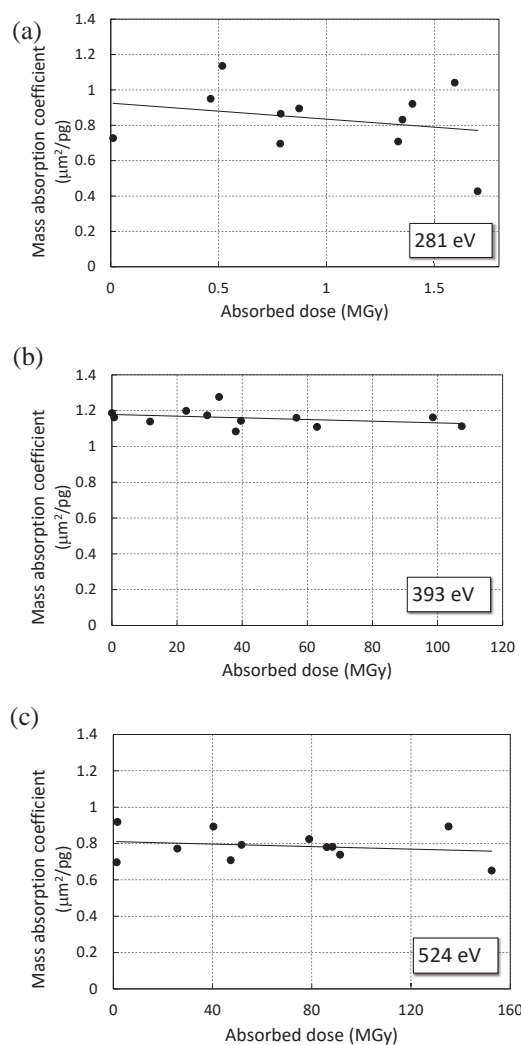


Fig. 1. Effects of soft X-rays on mass absorption coefficients in DNA at (a) C *K*, (b) N *K*, (c) O *K*-edges. The solid lines show linear regression.

- [1] K. Shinohara *et al.*, *Ultramicrosc.* **194** (2018) 1.
- [2] K. Shinohara *et al.*, *J. X-Ray Sci. Technol.* **26** (2018) 877.
- [3] K. Shinohara *et al.*, *Cells* **8** (2019) 8.
- [4] A. Ito *et al.*, *UVSOR Activity Report* **49** (2021) 152.

Attempt to Constrain the Initial Condition of Aqueous Alteration on Cometary Organic Matter

H. Yabuta¹, N. Nishii¹, T. Araki² and H. Yuzawa²

¹Department of Earth and Planetary Systems Science, Hiroshima University, Kagamiyama 1-3-1, Hiroshima 739-8526 Japan

²UVSOR Synchrotron Facility, Institute for Molecular Science, Okazaki 444-8585, Japan

This study aims to understand the chemical evolution of organic matter in the early stage of aqueous alteration of icy small bodies, through the freeze-thaw experiment of analogues of cometary organic matter.

As a starting material, HCN polymer was synthesized by heating formamide (0.3 ml) at 185°C for 72 hours [1]. The HCN polymer in the same volume of Milli-Q water was frozen with liquid nitrogen (-196°C), kept in the freezer (-18°C), and thawed under room temperature. This freeze-thaw cycle experiment was conducted 10, 20, 30, and 40 cycles. Each experimental products were filtered to remove the residual formamide and once dried.

For the scanning transmission x-ray microscopy (STXM) measurements, each experimental products were suspended in methanol and dropped in SiO₂-supported Cu transmission electron microscopy (TEM) grids. C- and N-XANES spectra of the samples were acquired by STXM-XANES, beamline 4U, UVSOR. Cody *et al.* (2008) [2] was referred to for the absorption peak assignment.

Figure 1 shows the C-XANES spectra of the products obtained from the freeze-thaw cycle experiments of HCN polymer. The spectrum of the starting material (0 cycle) contains the developed peak derived from nitrile or N-heterocycles with the other three peaks derived from aromatic carbon, carbonyls, and alcohol/ether. Except for the freeze-thaw 10 cycle product showing the high peaks of aliphatic and carbonyl carbons, the spectra of the other products are relatively similar to that of the starting material, but peak intensities of nitrile /N-heterocycles and carbonyls in the spectra of the freeze-thaw 30 and 40 cycles products are lower than those in starting material and the 20 cycle products. The result shows that HCN polymer is likely hydrolyzed and altered with the progress of low temperature freeze-thaw processes. In addition, the freeze-thaw 30 and 40 cycles products showed similar C-XANES spectra to those of ultracarbonaceous Antarctic micrometeorites

(UCAMM) [3], supporting the formation of the UCAMM with a very small amount of fluid on a cometary body.

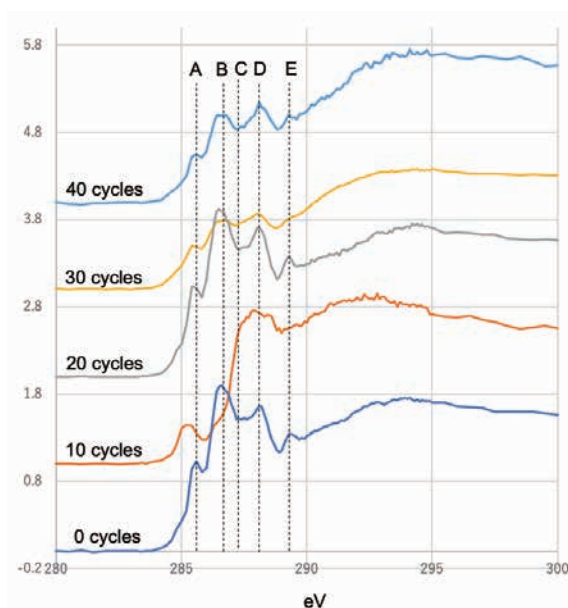


Fig. 1. C-XANES spectra of the products obtained from the freeze-thaw cycle experiments of HCN polymer (0, 10, 20, 30, and 40 cycles). Peak A: $1s-\pi^*$ transition for aromatic carbon ($C=C^*$) at 285.6 eV, peak B: $1s-\pi^*$ transition for nitrile ($C\equiv N^*$) or N-heterocycles ($C-N^*=C$), at 286.6 eV, peak C: $1s-3p/s^*$ transition for aliphatic carbon (CH_x) at 287.5 eV, peak D: $1s-\pi^*$ transition for carbonyl carbon ($OR(C^*=O)-C$) at 288.4–288.7 eV, and peak E: $1s-3p/s^*$ transition for alcohol or ether (CH_x-OR) at 289.3 eV.

[1] F. Cataldo, G. Patanè and G. Compagnini, *J. Macromol. Sci. Part A* **33** (2009) 1039.

[2] G. D. Cody *et al.*, *Meteorit. Planet. Sci.* **43** Nr 1/2 353.

[3] H. Yabuta, *et al.*, *Geochim. Cosmochim. Acta* **214** (2017) 172.

BL4U

Organics in Asteroid Ryugu Samples: Analytical Approach Utilizing Micro and Multi Beam Techniques.

M. Ito¹, N. Tomioka¹, M. Uesugi², A. Yamaguchi^{3,4}, N. Imae^{3,4}, N. Shirai⁵, T. Ohigashi^{4,6}, M. Kimura³, M-C, Liu⁷, R.C. Greenwood⁸, K. Uesugi², A. Nakato⁹, K. Yogata⁹, H. Yuzawa⁶, Y. Kodama⁸, A. Tsuchiyama¹⁰, M. Yasutake², R. Findlay⁸, I.A. Franchi⁸, J.A. Malley⁸, K.A. McCain⁷, N. Matsuda⁷, K.D. McKeegan⁷, K. Hirahara¹¹, A. Takeuchi², S. Sekimoto¹², I. Sakurai¹³, I. Okada¹³, Y. Karouji¹⁴, T. Yada⁹, M. Abe⁹, T. Usui⁹, S. Watanabe¹³ and Y. Tsuda^{4,9}
¹JAMSTEC Kochi, ²JASRI/SPring-8, ³NIPR, ⁴SOKENDAI, ⁵Tokyo Met. Univ.,
⁶UVSOR/IMS, ⁷UCLA, ⁸Open Univ., ⁹JAXA/ISAS, ¹⁰Ritsumeikan Univ.,
¹¹Osaka Univ., ¹²Kyoto Univ., ¹³Nagoya Univ., ¹⁴JAXA/JSEC, ⁵Toyo Corp.

How the Earth gained its water and organics remains an outstanding question in planetary science. While a small fraction may have been inherited from the cloud of gas and dust present when the Solar System formed, most was likely delivered to the inner Solar System region by water- and carbonaceous-rich materials i.e., asteroids, meteorites, interplanetary dust particles and comets that may be originated beyond the orbit of Jupiter. To better understand the origin of primitive water- and carbonaceous-rich asteroids, JAXA sent the Hayabusa2 spacecraft to asteroid Ryugu and returned surface and subsurface samples from it in December 2020.

In June 2021, following the initial characterization phase conducted at JAXA curation facility, a subset of Ryugu materials were the subject of investigations by separate research teams of six initial analysis and two curation teams [1-8]. Based on the investigations of bulk O isotopes, major elemental abundances and their mineralogical characteristics [1-3,9], the samples returned from Ryugu have shown that they closely match the rare, water rich, Ivuna type (CI) chondritic meteorites.

Analysis of the organic component in Ryugu particles has been a major theme during this first intensive phase of research activity. One of the successes of the work carried out on the Ryugu materials has been the identification of a clear relationship between coarse grained phyllosilicates and organics indicating of water-mineral-organics interaction under a reducing environment on the asteroid [1]. This was confirmed by a STXM (UVSOR-BL4U), NanoSIMS (JAMSTEC, Kochi) and TEM (JAMSTEC, Kochi) coordinated microanalysis [1]. Approximately 20,000 organic species consisting of carbon, hydrogen, nitrogen, oxygen, and/or sulfur, and at least 20 amino-acids have been identified by using high-sensitivity mass spectrometry [1,6,7]. Studies of chiral amino acids in Ryugu have shown that the abundance of the D- and L-enantiomers are approximately equal (D/L = 1),

indicating nonbiological origins [6]. The diversity of organic matter found in Ryugu samples shows some similarities with that previously reported in primitive carbonaceous chondrite groups [1,6,7].

Isotope analyses of the Ryugu particles have provided clues to the original provenance of these Ryugu-derived materials [1,10-12]. This indicates that materials from Ryugu display similarities to other postulated outer Solar System materials, including interplanetary dust particles, returned cometary materials and spectroscopic observations of comets. These results suggest that Ryugu, and by inference other type asteroid, could have formed in outer Solar System regions, such as are now occupied by Uranus and Neptune. A finding of CO₂-bearing water in a Ryugu pyrrhotite is also another evidence of outer Solar System origin [4]. Ryugu-like C-type asteroidal bodies may be present in the inner Solar System as a result of giant planet migration [13].

The success of the Hayabusa2 mission and subsequent analytical campaign [1-8] demonstrates the importance of using state-of-the-art analytical techniques when investigating spacecraft returned samples.

- [1] M. Ito *et al.*, *Nat. Astron.* **6** (2022) 1163.
- [2] E. Nakamura *et al.*, *Proc. Jpn. Acad., Ser. B* **98** (2022) 227.
- [3] T. Yokoyama *et al.*, *Science* **379** (2023) eabn7850.
- [4] T. Nakamura, *et al.*, *Science* **379** (2023) eabn8671.
- [5] R. Okazaki *et al.*, *Science* **379** (2023) eabo0431.
- [6] H. Naraoka *et al.*, *Science* **379** (2023) eabn9033.
- [7] H. Yabuta *et al.*, *Science* **379** (2023) eabn9057.
- [8] T. Noguchi *et al.*, *Nat. Astron.* **7** (2023) 170.
- [9] R. C. Greenwood *et al.*, *Nat. Astron.* **7** (2022) 29.
- [10] N. Kawasaki *et al.*, *Sci. Adv.* **8** (2022) eade2067.
- [11] D. Nakashima *et al.*, *Nat. Commun.* **14** (2023) 532.
- [12] T. Hopp *et al.*, *Sci. Adv.* **8** (2022) eadd8141.
- [13] A. Morbidelli, *et al.*, *Meteorit. Planet. Sci.* **35** (2000) 1309.

Chemical Morphology of Biomass-Burning Particles Generated from Different Fuels under Varied Burning Conditions

J. Chen¹, N. Faure², Y. Hao³, Z. Kanji¹, E. S. Thomson², S. Wang³ and X. Kong^{2*}

¹Institute for Atmospheric and Climate Science, ETH Zürich, Zurich, 8092, Switzerland

²Department of Chemistry and Molecular Biology, University of Gothenburg, SE-412 96 Gothenburg, Sweden

³Department of Environmental Sciences, College of Urban and Environmental Sciences, Northwest University, Xi'an 710127, China

Biomass burning aerosols (BBA) from fires worldwide have the potential to greatly disrupt the atmosphere-Earth climate system, as they directly absorb solar radiation and also indirectly affect the radiative properties of clouds. However, due to the intricate chemical composition of BBA produced from a variety of fuels under different burning conditions, the environmental and climatic repercussions of BBA remain highly uncertain.

In this study, BBA generated from laboratory burning experiments were examined by scanning transmission X-ray microscopy (STXM), in order to understand the factors influencing the chemical morphologies of BBA. Various types of biomasses (softwood, hardwood, leaves, peat) were burned under controlled conditions, including flaming and smoldering conditions. The generated BBA particles were transferred to the aerosol chamber and collected onto the TEM grid for chemical morphology analysis by. The STXM measurements were performed at the BL4U beamline in UVSOR-III [1].

The images of example particles are shown in Fig. 1, including the BBA particles from softwood under flaming condition (Fig. 1a), and softwood, peat, leaves BBA particles from smoldering condition (Fig. 1b-1d). The morphologies of particles varied between burning conditions: particles formed under flaming condition exhibit a chain-like structure (Fig. 1a), which is typical for fresh soot particles. As for particles collected under the smoldering condition (Fig. 1b-1d), they display a core-shell structure, implying a mixture of organics and soot particles.

The carbon K-edge near edge X-ray absorption fine structure (NEXAFS) spectra of individual particles from different cases were shown in Fig. 2, where the corresponding particles are displayed on the right. All spectra show the absorbance around 285 eV (arising from the $C\ 1s \rightarrow \pi^*_{R(C^*=C)R}$ transition) and a broader peak at 290 eV (attributing by $C\ 1s \rightarrow \sigma^*$ aromatic $C=C$ transitions). This is one of the identifying features of soot particles. Thus, the strong absorbance at 285 eV of wood-burning particles (softwood flaming and smoldering) indicates the origin of soot particles. This peak is relatively lower in peat and leaves smoldering cases, implying less contributions from soot particles. Two specific peaks at 297.1 eV and 299.8 eV due to the transitions of $K\ L2\ 2p_{1/2} \rightarrow \sigma^*$ and $K\ L2\ 2p_{3/2} \rightarrow \sigma^*$ were observed in the leaves smoldering case. The spectra feature in the energy range from 285 eV to 290 eV varied with samples, which is associated with oxygen-

containing organic functional groups and needs further investigation.

These results show that the BBA has distinct chemical morphology depending on biomass types and burning conditions, and the STXM serves as a useful tool to study the morphology and chemical natures of these BBA particles.

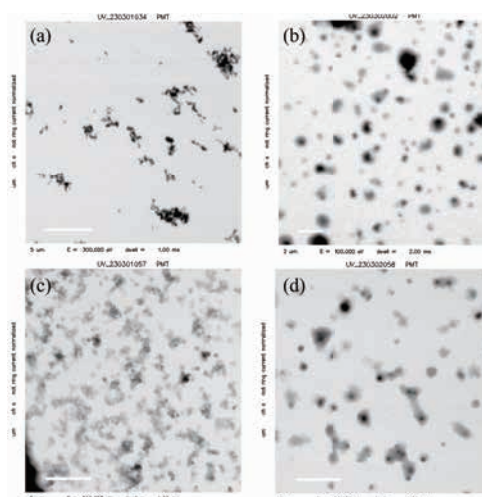


Fig. 1. The morphology of BBA particles from burning different biomasses: (a) Softwood burned under flaming condition; (b-d) softwood, peat and leaves burned under smoldering conditions, respectively. The used photon energy was 300 eV.

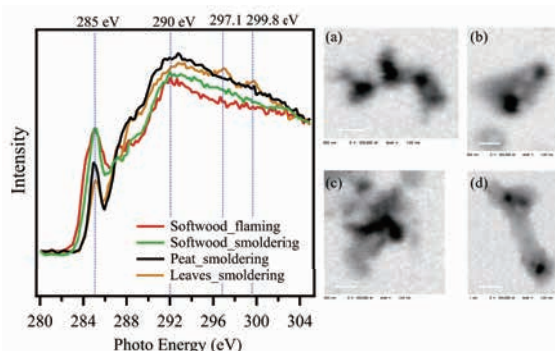


Fig. 2. Left: NEXAFS C K-edge spectra of example particles. Right: (a) softwood burned under flaming condition; (b-d) softwood, peat and leaves burned under smoldering conditions, respectively.

[1] T. Ohigashi *et al.*, J. Phys. Conf. Ser., **463** (2013) 012006.

BL5B

Heat Resistance of SiC/Mo/Si Multilayer Mirrors at 30.4nm

S. Teramoto², K. Inoue¹, A. Yamazaki¹, T. Matsumoto², S. Liu², K. Yoshioka^{1,2} and I. Yoshikawa^{1,2}

¹Development of Earth and Planetary Science, Graduate School of Science,
The University of Tokyo, Tokyo 113-0033, Japan

²Development of Complexity Science and Engineering, Graduate School of Frontier Sciences,
The University of Tokyo, Chiba 277-8561, Japan

Optical observations of planetary atmospheres are conducted over a wide range of wavelengths. In particular, ultraviolet light is useful for obtaining various information about planetary upper atmospheres. For example, by detecting the emission of He II (30.4 nm), the distribution of plasma surrounding the Earth can be observed. The behavior of plasma is related to solar activity and is the key to understanding the physics and evolution of the environment within the solar system. However, the problem is that the signal-to-noise ratio is small due to the low light intensity in UV observations.

Therefore, technology using periodic multilayer for the normal incidence optics in the EUV wavelength ranges has been developed for many planetary science missions, such as Nozomi [1], Kaguya, and EQULEUS [2]. The normal incidence optics is necessary to determine the distribution of plasma. However, the problem is that the normal incidence optics have low reflectance. We can solve this problem by using multilayer mirrors.

Multilayer mirrors can dramatically improve reflectance due to the interference of reflected light at each interface. In particular, the development of high-reflectance multilayer mirrors for He II radiation at 30.4 nm is progressing. A Mo/Si mirror is widely used due to its high stability.

Previously, we demonstrated the performance of a new multilayer mirror consisting of 40 pairs of Mg and SiC, achieving a maximum reflectivity of over 30%. However, it was found that the Mg/SiC mirror had a critical flaw. The reflectivity decreases in high-temperature and high-humidity environments. In actual observations, multilayer mirrors are exposed to high-temperature and humid environments before launch and extremely cold environments in space. Therefore, it is necessary to develop observation equipment that is resistant to such environmental changes.

Since a combination of Mo/Si is stable [3], we designed a new multilayer mirror (SiC/Mo/Si). The new mirror is manufactured by depositing the three different materials periodically. To evaluate its resistance to high-temperature environments, we

conducted a heat environment test in a constant-temperature oven (50 degrees Celsius for 24 hours) and compared the reflectances of the mirrors before and after heating.

The synchrotron radiation was spectroscopic with G3M5. It was led to the calibration chamber. EUV light was irradiated onto the multilayer mirror, and its wavelength dependence was evaluated. The measurement was conducted three times.

Fig. 1 shows the reflectances for the S-polarization of the mirror before and after high-temperature exposure (50 degrees Celsius for 24 hours). The reflectance decreased by approximately 5% after the high-temperature exposure. The irregularity of the interface may have affected the result.

In the future, changing the manufacturing process will make it possible to create a more stable mirror with higher reflectance. We plan to improve the performance of the mirror that is more resistant to environmental changes and have higher reflectance in the next year.

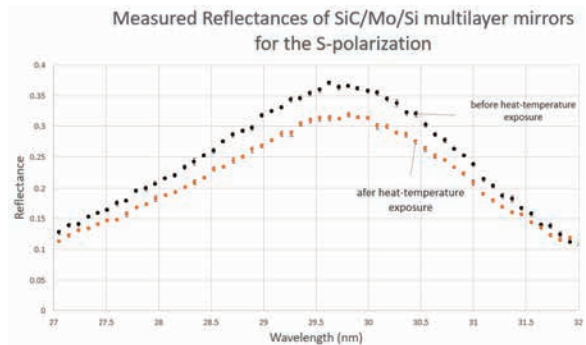


Fig. 1. Reflectances of SiC/Mo/Si mirrors before (black dots) and after (orange dots) heat-temperature exposure.

[1] I. Yoshikawa *et al.*, *Earth Planets Space* **60** (2008) 407.

[2] M. Kuwabara *et al.*, *JAXA Research and Development Report* (2019).

[3] L. Yunpeng *et al.*, *Appl. Surf. Sci.* **317** (2014) 902.

Synchrotron-radiation Infrared Microspectroscopy Analysis of Persistent Organic Compounds

T. Kawasaki¹, F. Teshima² and K. Tanaka²

¹Accelerator Laboratory, High Energy Accelerator Research Organization, Tsukuba 305-0801, Japan

²UVSOR Synchrotron Facility, Institute for Molecular Science, Okazaki 444-8585, Japan

It is important for absorption of carbon dioxide under atmosphere to manage woody biomass properly. Lignin is a part of ingredients of woods and is composed of many phenolic compounds. It has been known that those aromatic molecules such as coumaryl alcohol and coniferyl alcohol are useful for functional materials. However, it is usually difficult to degrade the lignin construct unless using strong acids with extremely high temperatures. We have found that soluble lignin that was prepared by alkaline treatment can be degraded to produce several aromatic molecules by using infrared free electron laser (IR-FEL) [1]. In this study, an insoluble sulfonated lignin was tested as another model sample for degradation by IR-FEL and far-infrared ray from gyrotron [2]. After those irradiations, the complex structure of the lignin was analyzed by using synchrotron-radiation infrared microspectroscopy. The measurement was performed by reflection mode with 64 scans.

In the FT-IR spectra of lignin in the far-infrared region (Fig. 1, upper), increases of absorption intensity can be observed from 150 to 250 cm^{-1} in all of samples. The inclinations in the cases of samples after the IR-FEL irradiations at 7.1 μm and 3.5 μm are similar with the case of the sample before irradiation (Non-irradiation). On the other hand, the irradiation by a submillimeter wave at 1.4 mm from gyrotron gave increase of absorption at 150-200 cm^{-1} . This may indicate that the hydration of the lignin sample can be occurred by the irradiation at longer wavelengths.

In the absorption spectra at mid-infrared region (Fig. 1, bottom), broad bands at 1000-1100 cm^{-1} can be observed in all of samples. Especially, another peak can be slightly detected after irradiations at 1.4 mm and 7.1 μm compared to that at 3.5 μm and the non-irradiation sample (dotted line). This region contains carbon-oxygen stretching vibrational modes, and the lignin is constructed by many ether bonds (C-O-C). Therefore, it can be considered that the structure of lignin can be modified and partial cleavage of the ether bonds can be induced by the submillimeter wave and the IR-FEL irradiations. We are planning to perform mass analysis to confirm the structural modification of the lignin.

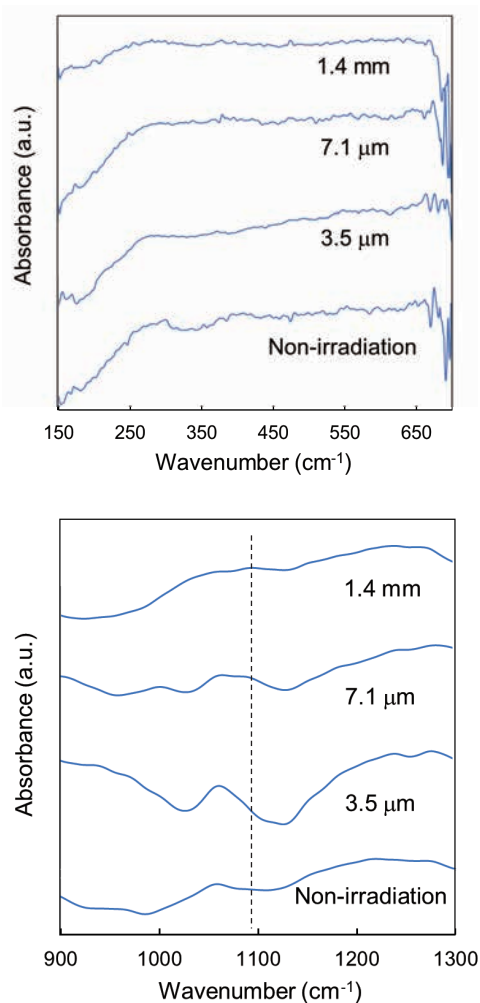


Fig. 1. Infrared absorption spectra of lignin in the far- (upper) and mid- (bottom) infrared regions. “1.4 mm” means the wavelength of submillimeter wave from gyrotron. Both of “7.1 μm ” and “3.5 μm ” are wavelengths of IR-FELs.

[1] T. Kawasaki *et al.*, *Polymers* **14** (2022) 2401.

[2] T. Kawasaki *et al.*, *Biomolecules* **12** (2022) 1326.

BL6B

Development of an Infrared Spectro-Microtomography Using a Mid-IR Supercontinuum Laser: Preliminary Report

H. Yabuta¹, Y. Ikemoto², F. Teshima³ and K. Tanaka³

¹*Department of Earth and Planetary Systems Science, Hiroshima University, Kagamiyama 1-3-1, Hiroshima 739-8526 Japan*

²*Japan Synchrotron Radiation Research Institute (JASRI) 1-1-1, Kouto, Sayo-cho, Sayo-gun, Hyogo 679-5198 Japan*

³*UVSOR Synchrotron Facility, Institute for Molecular Science, Okazaki 444-8585, Japan*

This study aims to develop a three-dimensional infrared spectro-microtomography using a mid-infrared supercontinuum laser, for investigating the three-dimensional spatial distributions of micron-sized organic materials and hydrous minerals of extraterrestrial samples and for understanding the chemical history in the early Solar System.

In the previous beamtime, an alignment procedure has been established to guide the laser source to the microscope for micro-spectroscopy. The activities of this beamtime were the following three points. The first was to adjust the beam size at the microscope focal point, the second was to confirm the sample holding technique, and the third was to confirm the IR imaging measurement technique by rotating the sample. The details are described in this order.

Fig. 1 shows the schematic illustration of the optical path. The IR beam emitted from the laser are reflected by BaF₂ and reduced to about 1/100 of its original intensity. The IR beam is further attenuated through an ND filter to an intensity that does not damage the optical components of the FTIR spectrometer, and then a spectrum is measured. The microscope at BL6B has 16 elements HgCdTe (MCT) linear array detector. In previous experiments, it was found that due to the small source size, the IR spot on the microscope was small and the IR light was only on a part of the element. In order to increase the number of elements that are illuminated by IR light, a beam expander was installed in front of the FTIR to adjust the spot size.

Samples are glued to the tip of a glass capillary and mounted on a goniostage. Figure 2(a) shows a photograph of the goniostage mounted on the microscope. Figure 2(b) shows a micrograph of a sample glued to the tip of the capillary. The sample was a milled breadcrumb and the size was approximately 90 micrometers in longitudinal.

In the previous beamtime, the mapping measurements were performed in the multipoint measurement mode of microscopy programs, but there is a problem of not being able to access integral intensity plots. In addition, the program is not equipped with a mode to extract only the part of the linear array detector that are illuminated by IR light. The element shift mapping software solves these problems and is used for the measurement.

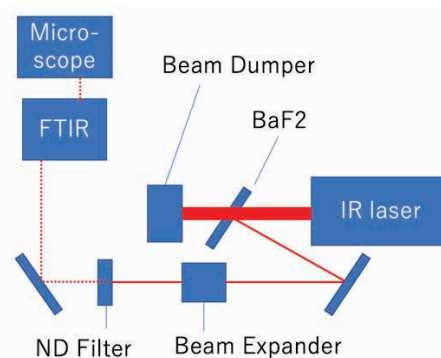


Fig. 1. Schematic illustration of the optical path

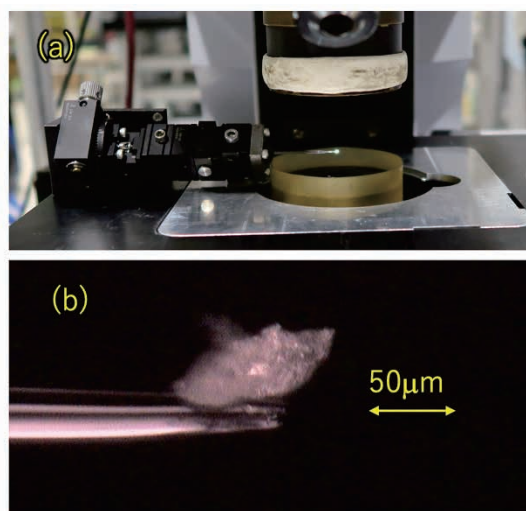


Fig. 2. (a) Photograph of the goniostage mounted on the microscope. (b) Micrograph of a sample glued to the tip of the capillary.

UVSOR User 8

